Temporal dynamics and chaotic intermittency in nonlinear wave-wave interactions in space plasmas

Rodrigo A. Miranda, Abraham C.-L. Chian, Erico L. Rempel, Instituto Nacional de Pesquisas Espaciais INPE, Brazil.

Copyright 2005, SBGf - Sociedade Brasileira de Geofísica

This paper was prepared for presentation at the 9th International Congress of the Brazilian Geophysical Society held in Salvador, Brazil, 11-14 September 2005.

Contents of this paper were reviewed by the Technical Committee of the 9th International Congress of the Brazilian Geophysical Society. Ideas and concepts of the text are authors' responsibility and do not necessarily represent any position of the SBGf, its officers or members. Electronic reproduction or storage of any part of this paper for commercial purposes without the written consent of the Brazilian Geophysical Society is prohibited.

Abstract

A nonlinear model of three-wave interactions and its temporal evolution is studied. First, we revise the techniques used to obtain the model. Starting from the MHD equations, we found an electrostatic expression for the Zakharov equations, which in the static approximation yield to the Nonlinear Schrödinger equation. The model is finally obtained using a three traveling wave truncation consisting in one linearly unstable pump wave and two linearly damped daughter waves. Then we proceed with the nonlinear dynamics analysis by constructing a bifurcation diagram, where we found a period-3 window. Examples of intermittency driven by temporal chaos present in the time series are shown. Some reviews of in-situ experiments and observations related to wave-wave interactions, and the relevance of the studied model are discussed.

Introduction

Observational evidence of wave-wave interactions have been reported in a number of in-situ experiments. For example, Boehm et al. (1990) detected a correlation of Langmuir, whistler and Alfvén waves in two rocket experiments in the auroral ionosphere over Alaska and Greenland. Gurnett et al. (1993) obtained observational evidence of three-wave interactions involving pump and daughter Langmuir waves and daughter ion-acoustic waves from wideband plasma measurements on the Galileo spacecraft, and the detection of type-III radio burst from a solar flare event. Stasiewicz et al. (1996) found evidence of interactions between Langmuir and lower-hybrid waves that are consistent with parametric decay of beam-induced Langmuir waves, as well as scattering of Langmuir waves on preexisting lower-hybrid waves, in observations from the Freja satellite. McAddams et al. (1999) reported the observation of high frequency emissions in the auroral ionosphere, and proposed that changes in the plasma density would induce the decay of Langmuir waves into a whistler mode wave, and the generation of the emissions observed. Recently, Deng et al. (2004) reported the crossing of the Geotail satellite with an active reconnection diffusion region in the Earth's magnetotail, where tailward electron beams aligned with the magnetic field and directed away from the X reconnection point excite Langmuir waves which were detected simultaneously with fluctuations of the magnetic field.

Over the years, a number of theoretical models of nonlinear wave-wave interactions had been proposed. Russell and Ott (1981) derived a system of nonlinear ordinary differential equations (ODEs) from a truncation of the Nonlinear Schrödinger (NLS) equation with linear growth rate and damping into three waves. Later, Gosh and Papadopoulos (1987) found the same set of ODEs deriving it from the derivative nonlinear Schrödinger (DNLS) equation, which is a version of the NLS equation with a derivative in the nonlinear term. Chian and Abalde (1997) studied the decay of a Langmuir pump wave into electromagnetic, Langmuir and ion-acoustic waves via hybrid stimulated modulational instability. Starting from the Zakharov equations, which describe the coupling of Langmuir, high-frequency electromagnetic and low-frequency ion-acoustic waves, and using a Fourier analysis they found coupled mode equations for the processes $L_0 \rightarrow T^+ + L^- + S$, $L_0 \rightarrow T^- + L^+ + S$ for the linear theory, and $L_0 \leftrightarrow T^+ + L^- + S$, $L_0 \leftrightarrow T^- + L^+ + S$ for the nonlinear theory.

In this paper we extend the work of Russell and Ott (1981) by numerical simulations of their system of ODEs. First, we present an overview of the derivation of the nonlinear (cubic) coupled set of ODEs. Then, in the next section we proceed to analyze its temporal dynamics by constructing a bifurcation diagram, choosing the magnitude of the wave growth/damping rate as the control parameter, and selecting a region of interest where a periodic window is created from the result of a saddle-node bifurcation, and is destroyed by an interior crisis. We demonstrate the occurrence of two types of intermittency in the time series obtained from the numerical simulations, and characterize them by means of power spectra. This work can improve our understanding on the intermittency phenomenon, which is frequently found in observational time series in active experiments in space plasmas.

Model equations

Starting from the continuity, the two-fluids and Maxwell equations:

$$\frac{\partial \mathbf{V}_\alpha}{\partial t} + (\mathbf{V}_\alpha \cdot \nabla) = \frac{q}{m}(\mathbf{E} + \mathbf{V}_\alpha \times \mathbf{B}) - \nu_\alpha \mathbf{V}_\alpha - \frac{\gamma_\alpha K_B T_\alpha \nabla n_\alpha}{n_\alpha m_\alpha} \quad (1)$$

$$\frac{\partial n_\alpha}{\partial t} + \nabla \cdot (n_\alpha \mathbf{V}_\alpha) = 0 \quad (2)$$

$$\nabla \times \mathbf{E} = -\frac{\partial \mathbf{B}}{\partial t} \quad (3)$$

$$\nabla \times \mathbf{B} = \mu_0 \mathbf{J} + \frac{1}{c^2}\frac{\partial \mathbf{E}}{\partial t} \quad (4)$$

$$\nabla \cdot \mathbf{E} = \frac{\rho}{\varepsilon_0} \quad (5)$$

$$\nabla \cdot \mathbf{B} = 0 \quad (6)$$

, and considering that the physical variables have two time-scales (i. e. high frequency fields oscillating near the electron plasma frequency, and low frequency fields oscillating below the ion cyclotron frequency) we have the following expressions for electronic density, ion density, velocity, current and electric field:

$$\begin{aligned} n_e &= n_0 + n_l + n_h \\ n_i &= n_0 + n_l \\ \mathbf{V}_e &= \mathbf{V}_l + \mathbf{V}_h \\ \mathbf{J} &= \mathbf{J}_l + \mathbf{J}_h \\ \mathbf{E} &= \mathbf{E}_l + \mathbf{E}_h \end{aligned}$$

, where the subscript *h* stands for high-frequency scale, *l* for low-frequency scale, and 0 represent the unperturbed condition for the corresponding variable.

Introducing the above time scales into equations (1) – (6) we obtain the Zakharov equations:

$$\frac{\partial^2 \mathbf{E}_h}{\partial t^2} + \omega_{pe}^2 \mathbf{E}_h - \gamma_e \mathbf{V}_{th}^2 \nabla (\nabla \cdot \mathbf{E}_h) = \omega_{pe}^2 \frac{n_{el}}{n_0} \mathbf{E}_h \quad (7)$$

$$\frac{\partial^2 n_{el}}{\partial t^2} - V_s^2 \nabla^2 n_{el} + \nu_i \frac{\partial n_{el}}{\partial t} = \frac{1}{2} \frac{\varepsilon_0}{m_i} \langle E_h \rangle^2 \quad (8)$$

which describe the nonlinear interaction between high frequency Langmuir waves and low frequency ion-acoustic waves, considering electrostatic waves only (i. e. longitudinal waves).

Now considering a collection of linear Langmuir waves in one spatial dimension whose electric field can be written as:

$$E_h(x,t) = \frac{1}{2} \tilde{E}(x,t) \exp(-i\omega_{pe} t) + c.c. \quad (9)$$

and defining the following dimensionless variables

$$\begin{aligned} \eta &= \frac{\gamma_e K_B T_e + \gamma_i K_B T_i}{K_B T_e} \\ z &= \left(\frac{2}{\gamma_e}\right) \left(\frac{\eta m_e}{m_i}\right)^{1/2} \left(\frac{x}{\lambda_D}\right) \\ \tau &= \left(\frac{2}{\gamma_e}\right) \left(\frac{\eta m_e}{m_i}\right) \omega_{pe} t \end{aligned}$$

so the following differential operators are defined as:

$$\begin{aligned} \frac{\partial}{\partial z} &= \left(\frac{\gamma_e}{2}\right) \left(\frac{m_i}{\eta m_e}\right)^{1/2} \lambda_D \frac{\partial}{\partial x} \\ \frac{\partial}{\partial \tau} &= \left(\frac{\gamma_e}{2}\right) \left(\frac{m_i}{\eta m_e}\right) \frac{1}{\omega_{pe}} \frac{\partial}{\partial t} \end{aligned}$$

, and also defining dimensionless variables for the electric field and density:

$$\begin{aligned} E &= \left(\frac{1}{\eta}\right) \left(\frac{m_i}{m_e}\right)^{1/2} \left(\frac{\gamma_e \varepsilon_0 \tilde{E}^2}{8 n_0 K_B T_e}\right)^{1/2} \\ n &= \left(\frac{\gamma_e}{4}\right) \left(\frac{m_i}{m_e \eta}\right) \left(\frac{n_{el}}{n_0}\right) \end{aligned}$$

the set of equations (7) – (8) becomes

$$i \frac{\partial E}{\partial \tau} + \frac{\partial^2}{\partial z^2} E = n E \quad (12)$$

$$\frac{\partial n}{\partial \tau} - \frac{\partial^2 n}{\partial z^2} = \frac{\partial^2}{\partial z^2} |E|^2 \quad (13)$$

Considering a static approximation in equation (13) we get $\partial n/\partial \tau = 0$, then the first term on the left of (13) vanishes. Integrating twice and setting the constants of integration equal to zero yield (Nicholson, 1983):

$$n = -|E|^2$$

, so that (12) becomes

$$i \frac{\partial E}{\partial \tau} + \frac{\partial^2 E}{\partial z^2} + |E|^2 E = 0 \quad (14)$$

which is called the nonlinear Schrödinger equation because it resembles the quantum mechanical Schrödinger equation. This is the starting point for Russell and Ott (1981), where a term representing linear wave growth/damping is included:

$$i \left(\frac{\partial E}{\partial t} + \hat{\gamma} E \right) + \frac{\partial^2 E}{\partial z^2} + \left(|E|^2 - |E|_0^2 \right) E = 0 \quad (15)$$

, and the term $|E|_0^2$ denoting the spatial average of $|E|^2$. Equation (15) is then approximated to a solution consisting of three traveling waves:

$$\begin{aligned} E(z,t) &= E_0(t) \exp[i(k_0 z - \omega_0 t)] \\ &\quad + E_1(t) \exp[i(k_1 z - \omega_1 t)] + E_2(t) \exp[i(k_2 z - \omega_2 t)] \end{aligned} \quad (16)$$

where the resonant condition $2k_0 = k_1 + k_2$, the linear dispersion $\omega_\sigma = k_\sigma^2$ ($\sigma = 0, 1, 2$) and the phase difference $\omega_{1,2} - \omega_0 = \delta_{1,2}$ are assumed.

Introducing (16) in (15), and taking the $k_{0,1,2}$ components we obtain the following set of complex ODEs:

$$\begin{aligned} \dot{E}_0 &= -\gamma(k_0) E_0 + i[|E_0|^2 E_0 + 2|E_1|^2 E_0 + 2|E_0|^2 E_0 \\ &\quad + 2\bar{E}_0 E_1 E_2 \exp(2i\delta t)] \end{aligned} \quad (17)$$

$$\begin{aligned} \dot{E}_1 &= -\gamma(k_1) E_1 + i[|E_1|^2 E_1 + 2|E_0|^2 E_1 + 2|E_2|^2 E_1 \\ &\quad + E_0^2 \bar{E}_2 \exp(-2i\delta t)] \end{aligned} \quad (18)$$

$$\begin{aligned} \dot{E}_2 &= -\gamma(k_2) E_2 + i[|E_2|^2 E_2 + 2|E_0|^2 E_2 + 2|E_1|^2 E_2 \\ &\quad + E_0^2 \bar{E}_1 \exp(-2i\delta t)] \end{aligned} \quad (19)$$

where the dot denotes temporal differentiation, and $\delta = (\delta_1 + \delta_2)/2$. This set of equations can be rewritten using the representation $E_{0,1,2} = a_{0,1,2}(t) \exp(i\psi_{0,1,2}(t))$ (where a e ψ are real amplitude and phase, respectively) to a new set of four real equations:

$$\begin{aligned} \dot{a}_0 &= \gamma_0 a_0 + 2 a_0 a_1 a_2 \sin\theta \\ \dot{a}_1 &= -\gamma_1 a_1 - a_0^2 a_2 \sin\theta \\ \dot{a}_2 &= -\gamma_2 a_2 - a_0^2 a_1 \sin\theta \\ \dot{\theta} &= -2\delta + a_1^2 + a_2^2 - 2a_0^2 \\ &\quad + \left[4 a_1 a_2 - a_0^2 \left(\frac{a_2}{a_1} + \frac{a_1}{a_2} \right) \right] \cos\theta \end{aligned}$$

where $\theta(t) = 2\psi_0 - \psi_1 - \psi_2 - 2\delta t$, $\gamma_0 = -\gamma(k_0)$, $\gamma_{1,2} = \gamma(k_{1,2})$. Following Russell and Ott (1981), we normalize the system so that $\gamma_0 = 1$, and assume that $\gamma_2 = \gamma_1 = \gamma$ (e. g.

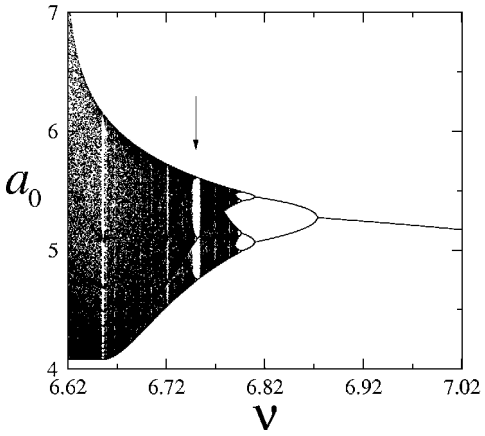

Figure 1 - Bifurcation diagram for a_0 as a function of the growth/damping rate ν. The arrow denotes the periodic window of interest.

consider Landau damping of the sidebands in the case of an even electron velocity distribution function) and the amplitudes $a_1 = a_2$. In this case the above four real equations are reduced to three:

$$\dot{a}_0 = a_0 + 2a_0a_1^2\sin\theta \quad (25)$$

$$\dot{a}_1 = -\gamma a_1 - a_0^2a_1\sin\theta \quad (26)$$

$$\dot{\theta} = -2\delta + 2(a_1^2 - a_0^2) + 2(2a_1^2 - a_0^2)\cos\theta \quad (27)$$

Note that the choice of signs for $\gamma_{0,1,2}$ indicates that wave 0 (i. e. the pump wave) is linearly unstable and its decay wave products are linearly damped.

Nonlinear analysis

The dynamics of the system (25) – (27) can be studied with the aid of a bifurcation diagram. Following previous notations from our group, we made $\gamma = \nu$ and set it as the control parameter, fixing δ = -6 arbitrarily. The set of equations (25) – (27) were numerically integrated, and the points where the orbit cuts the Poincaré surface defined by $a_1 = 1$, with da_1/dt > 0 (i. e. from "left" to "right") are plotted, after ignoring the initial transient.

Figure 1 shows a bifurcation diagram for a_0 as a function of ν, which demonstrates the rich dynamical behavior of the system. Figure 1 shows the occurrence of simple limit cycle, and a cascade of period doubling bifurcations from right to left, leading to chaos, which is occasionally interrupted by periodic windows. We focus our attention at the periodic window marked by an arrow, for which we construct a detailed bifurcation diagram showed in fig. 2(a)

From figure 2(a) we can see that the periodic window is created after a saddle-node bifurcation in $\nu = \nu_{SNB}$ = 6.7547 (marked as SNB), where a period-3 stable periodic orbit (SPO) and a period-3 unstable periodic orbit (UPO) are created. As ν decreases, the SPO evolves to a period-6 orbit, then to a period-12 orbit, and so on. Eventually, this cascade of period doubling bifurcations leads to a three-band weak chaotic attractor. At $\nu = \nu_{IC}$ = 6.7469, an abrupt enlargement of the banded chaotic attractor occurs in an event known as interior crisis where the banded chaotic attractor collides with the

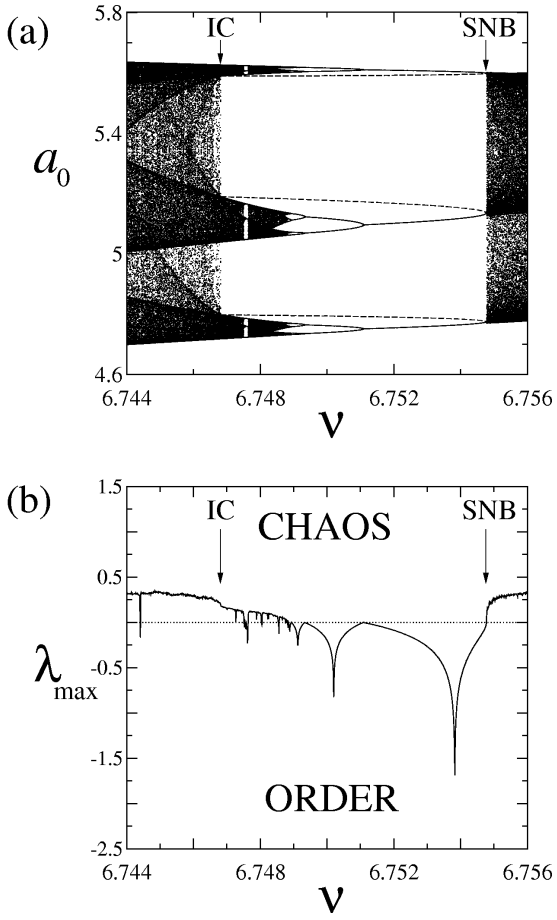

Figure 2 - (a) Enlargement of the bifurcation diagram showing the period-3 window; the dashed lines denotes the period-3 mediating UPO, SNB denotes saddle-node bifurcation and IC denotes interior crisis; (b) maximum Lyapunov exponent λ_{MAX} as a function of ν.

mediating unstable periodic orbit, resulting in an enlargement of the chaotic attractor (Grebogi et al, 1983), marked as IC in figure 2(a). Figure 2(b) shows the value of the maximum Lyapunov exponent λ_{MAX} corresponding to each value of ν. Considering that $\lambda_{MAX} > 0$ is a signature of chaotic behavior, while $\lambda_{MAX} < 0$ corresponds to periodic behavior, figure 2(b) is in agreement with fig 2(a). The saddle-node bifurcation and the interior crisis events are manifested as discontinuities in the values of λ_{MAX} in figure 2(b). Note that, during the cascade of period duplication of the SPO, when $\lambda_{MAX} = 0$ a bifurcation occurs.

Figure 3 shows the transition from order to chaos at the saddle-node bifurcation. At ν = 6.7547 the time series (fig 3(a)) and the Poincaré points (fig. 3(b)) show periodic behavior. Fig. 3(c) shows the power spectrum for the time series from fig. 3(a), in log-log scale. The periodic behavior is reflected by the occurrence of discrete peaks. At ν = 6.7548 the time series (fig. 3(d)) shows the occurrence of intermittency known as type-I Pomeau-Manneville intermittency (Pomeau and Manneville, 1980), which can be seen at the Poincaré points of fig3(e) represented by "bursts" interrupting laminar periods that

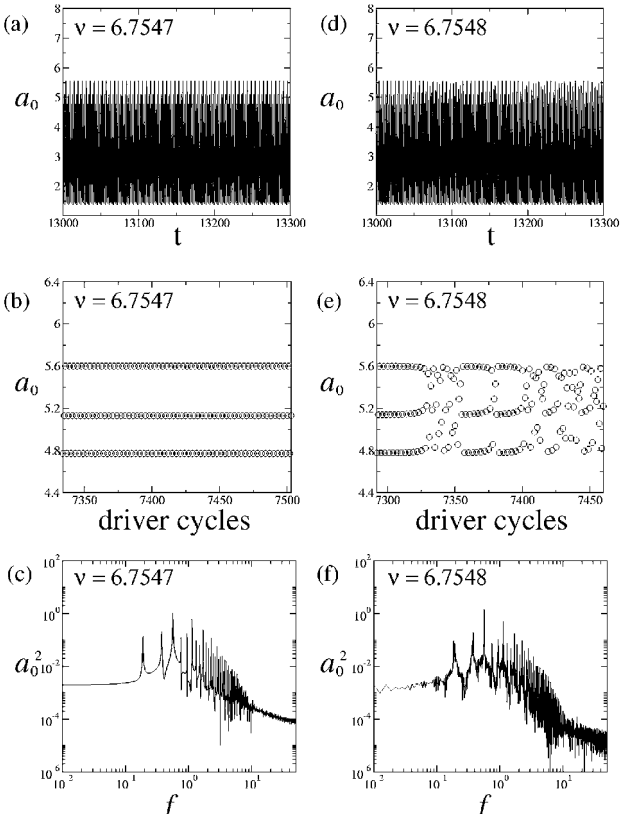

Figure 3 - Transition from order to chaos in the saddle-node bifurcation region; (a) time series of a_0 and (b) their Poincaré points at the period-3 regime, (c) power spectrum of the time series in log-log scale; (d) time series of a_0 and (e) Poincaré points at the same interval but for $\nu > \nu_{SNB} = 6.7547$. (f) Power spectrum of the chaotic time series in log-log scale.

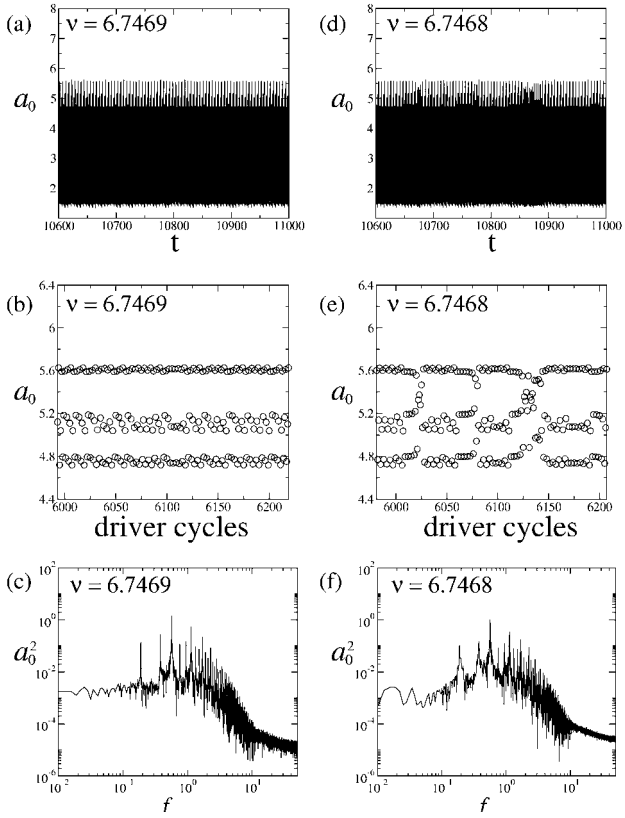

Figure 4 - Transition from weak chaos to strong chaos in the interior crisis region; (a) time series of a_0 and (b) their Poincaré points at the weak (banded) chaotic regime, (c) power spectrum of the time series in log-log scale; (d) time series of a_0 and (e) Poincaré points at the same interval but for $\nu < \nu_{IC} = 6.7469$. (f) Power spectrum of the chaotic time series in log-log scale.

resemble the previous period-3 orbit after the saddle-node bifurcation. The power spectrum shown in fig. 3(f) is now broad-band.

Another type of intermittency occurs at the interior crisis. Figure 4(a) shows a time series at $\nu > \nu_{IC} = 6.7469$, whose Poincaré points (fig. 4(b)) show no strong chaotic bursts, and the orbit stays confined in the region corresponding to the weak (banded) chaotic attractor. At $\nu = 6.7469$ the time series shows the crisis-induced intermittency, represented on the Poincaré points series (fig. 4(e)) as temporary "bursts" where the orbit corresponding to the pre-crisis chaotic attractor escapes to other regions of the phase space. Figs. 4(c) and 4(f) show the power-spectra for both cases in log-log scale. Note that the main peaks are observed at the pre-crisis and the post-crisis situations, but they are less pronounced in the latter case.

Discussion and concluding remarks

A set of real ordinary differential equations describing the nonlinear dynamics of three plasma waves in terms of their amplitudes were derived from the two-fluids motion equations, the continuity and the Maxwell equations. A more realistic model representing the physical situations described by the NLS equation may require to include additional modes resulting in a larger number of coupled ordinary differential equations. But for the case of weak instabilities, where higher modes of daughter waves are strongly damped, the truncation to just three terms can be justified. In this process the most restrictive assumption we made was to consider the amplitudes of the daughter waves as having the same value ($a_1 = a_2$) and the same growth/damping rate ($\gamma_1 = \gamma_2$). This allowed us to reduce our problem from four to three ODEs, simplifying the implementation of the numerical simulations.

We presented the occurrence of two types of intermittency commonly found in nonlinear systems: type-I Pomeau-Manneville and crisis-induced intermittency as we slightly modify the control parameter ν. Also, we reported changes over the power spectrum obtained from the times series during the transition from order to chaos, and from weak chaos to strong chaos.

The analysis presented here can improve our understanding of turbulent phenomena in space plasmas, since solar wind observations frequently display intermittent features. It is useful to compare the power spectra obtained from the numerical simulations and from in-situ observations. For example, Karlický and Bárta (2004) recently showed a power spectrum obtained from

solar radio emissions that have some similar structural characteristics with the ones obtained in this work.

Acknowledgments

The authors would like to thank an anonymous referee for his/her help in evaluating this paper. This work is supported by CAPES and CNPq.

References

Bohem, M. H., Carlson, C. W., McFadden, J. P., Clemmons, J. H., Mozer, F. S. High-resolution sounding rocket observations of large-amplitude Alfvén waves. J. Geophys. Res., Vol 95, pp. 1257-1271, 1990

Chian, A. C.-L., Abalde, J. R. Fundamental plasma radiation generated by a traveling Langmuir wave: hybrid stimulated modulational instability. J. Plasma Phys., Vol 57, Nº 4, pp. 753-763, 1997

Deng, X. H., Matsumoto, H., Kojima, H., Mukai, T., Anderson, R. R., Baumjohann, W., Nakamura, R. Geotail encounter with reconnection diffusion region in the Earth's magnetotail: Evidence of multiple X lines collisionless reconnection? J. Geophys. Res., Vol 109, A05206, 2004.

Gosh, S., Papadopoulos, K. The onset of Alfvénic turbulence. Phys. Fluids Vol 30, N^{o} 5, pp. 1371-1387, 1987.

Grebogi, C., Ott, E., Yorke, J. A. Crises, sudden changes in chaotic attractors, and transient chaos. Physica D, Vol 7, 181-200, 1983.

Gurnett, D. A., Hospodarsky, G. B., Kurth, W. S., Williams, D. J., Bolton, S. J. Fine Structure of Langmuir Waves Produced by a Solar Event. J. Geophys. Res., Vol 98, N^{o} A4, pp. 5631-5637, 1993.

Karlický, M., Bárta, M. Diagnostics of solar flare reconnection. Non. Proc. In Geophys., Vol 11, pp. 471-483, 2004.

McAdams, K. L., LaBelle, J., Trimpi, M., L., Kintner, P. M., Arnoldy, R. A. Rocket observations of banded structure in waves near the Langmuir frequency in the auroral ionosphere. J. Geophys. Res. Vol 104, N^{o} A12, pp. 28109-28122, 1999.

Nicholson, D. R. Introduction to Plasma Theory. John Wiley & Sons, 1983.

Pomeau, Y., Manneville, P. Intermittent transition to turbulence in dissipative dynamical systems. Comm. In Math. Phys. Vol 74, 189-197, 1980.

Russell, D. A, Ott, E. Chaotic (strange) and periodic behavior in instability saturation by the oscillating two-stream instability. Phys. Fluids, Vol. 24, N^{o} 11, pp. 1976-1988, 1981.

Stasiewicz, K., Holback, B., Krasnoselskikh, V., Boehm, M., Boström, R., Kintner, P. M. Parametric instabilities of Langmuir waves observed by Freja. J. Geophys. Res., Vol 101, N^{o} A10, pp. 21515-21525, 1996.